processes

MDPI

Article

Separation of Ternary System 1,2-Ethanediol + 1,3-Propanediol + 1,4-Butanediol by Liquid-Only Transfer Dividing Wall Column

Yan-Yang Wu *, Zhong-Wen Song, Jia-Bo Rao, Yu-Xian Yao, Bin Wu, Kui Chen and Li-Jun Ji

School of Chemical Engineering, East China University of Science & Technology, Shanghai 200237, China; songzw.ecust@gmail.com (Z.-W.S.); chenkui@ecust.edu.cn (K.C.); jilijun@ecust.edu.cn (L.-J.J.)
* Correspondence: wyywitty@ecust.edu.cn

Abstract: This study focuses on separating a mixture consisting of 1,2-ethanediol (1,2-ED), 1,3-propanediol (1,3-PD), and 1,4-butanediol (1,4-BD). Vapor–liquid equilibrium (VLE) data for 1,2-ED + 1,4-BD and 1,3-PD + 1,4-BD are determined at 101.3 kPa using a modified Rose equilibrium still. The consistency of the VLE data is checked with both Redlich–Kister and Fredenslund tests. The VLE data are fitted by the Wilson, NRTL, and UNIQUAC activity coefficient models. All three models can effectively correlate the VLE data. Then, the separation of the mixture is designed with the NRTL model and its correlated binary interaction parameters. A liquid-only transfer dividing wall column (LDWC) is investigated on the basis of a direct conventional distillation sequence (DCDS). For a fair comparison, both DCDS and LDWC are optimized to minimize total annual cost using sequential iterative optimization procedures. After optimization, LDWC exhibits a 16.87% reduction in total annual cost, while cooling and heating utility consumptions are reduced by 28.40% and 19.24% compared to DCDS.

Keywords: vapor–liquid equilibrium; sequential iterative optimization; distillation; liquid-only transfer dividing column

check for updates

Citation: Wu, Y.-Y.; Song, Z.-W.; Rao, J.-B.; Yao, Y.-X.; Wu, B.; Chen, K.; Ji, L.-J. Separation of Ternary System 1,2-Ethanediol + 1,3-Propanediol + 1,4-Butanediol by Liquid-Only Transfer Dividing Wall Column. *Processes* **2023**, *11*, 3150. https://doi.org/10.3390/pr11113150

Academic Editor: Fausto Gallucci

Received: 29 September 2023
Revised: 29 October 2023
Accepted: 30 October 2023
Published: 4 November 2023

Copyright: © 2023 by the authors. Licensee MDPI, Basel, Switzerland. This article is an open access article distributed under the terms and conditions of the Creative Commons Attribution (CC BY) license (https://creativecommons.org/licenses/by/4.0/).

1. Introduction

Diols including 1,2-ethanediol (1,2-ED), 1,3-propanediol (1,3-PD), and 1,4-butanediol (1,4-BD) can be used as solvents, antifreeze, pharmaceutical synthesis, polyester intermediates, etc. [1]. They can be obtained through chemical synthesis or catalytic hydrocracking of sorbitol derived from bioconversion processes [2]. Separation and purification are the keys to their industrial application. Distillation, as the most widely applied separation technology [3], is considered in this article. As conventional distillation column normally consumes a large amount of energy [4–7], it is promising to find an alternative column configuration with lower energy consumption.

Dividing wall column (DWC) involving a vertical partition wall proposed by R.O. Wright can be one of the alternative column configurations [8]. It reduces the internal re-mixing of the feed stream and side-draw product [9], reducing energy consumption compared to the conventional distillation column. In addition, it saves capital costs by reducing one condenser and reboiler by integrating the main column and prefractionator into a single shell. Much research has been done on the DWC for ternary mixture separation. Kaibel [8] studied the performance of DWC to separate a mixture of n-octane, n-heptane, and n-hexane under an equimolar fraction feed. It showed that DWC can reduce about 20% of the energy consumption compared with direct conventional distillation sequence (DCDS). Kolbe and Wenzel [10] applied the DWC to petrochemical cuts and calculated its capital cost. Approximately 20% of capital cost can be saved, along with higher capacity compared to DCDS. Ling et al. [11] investigated the controllability of the benzene, toluene, and o-xylene DWC through a four-column equivalent model. It demonstrated that product purity can be controlled by manipulating reflux ratio, side-product flow, liquid split, and ratio reboiler duty with a tiny purity deviation. However, only about 200 DWCs

have been built globally [12]. Effectively controlling the vapor split ratio [13], which substantially impacts product purity, capital cost, and energy consumption, is one of the DWC application's constraints.

To eliminate the vapor split ratio, Agrawal proposed a new alternative configuration named the liquid-only transfer DWC (LDWC) [13], shown in Figure 1. Ramapriya and Agrawal [13] have demonstrated that LDWC is equivalent to DWC through physical reasoning. Cui et al. [14] investigated ten different liquid-only transfer topologies that could separate the equimolar mixture of benzene, toluene, and m-xylene. These topologies included DCDS and LDWC. The simulation results showed that LDWC could save economic and energy consumption compared to the other nine topologies. Based on the static state study, Cui et al. [15] investigated LDWC dynamic control performance for the ternary mixture separation. The product purity could be maintained using five temperature controllers with an additional internal composition controller when handling ±20% disturbance in feed flow or composition. Furthermore, Zhang et al. [16] focused on the dynamic control of LDWC for the separation of an equimolar quaternary mixture. Their work showed that LDWC can be easily controlled well only using temperature controllers facing ±15% disturbance. LDWC provides a new path for DWC's application. So, it is used to separate the diols in this study.

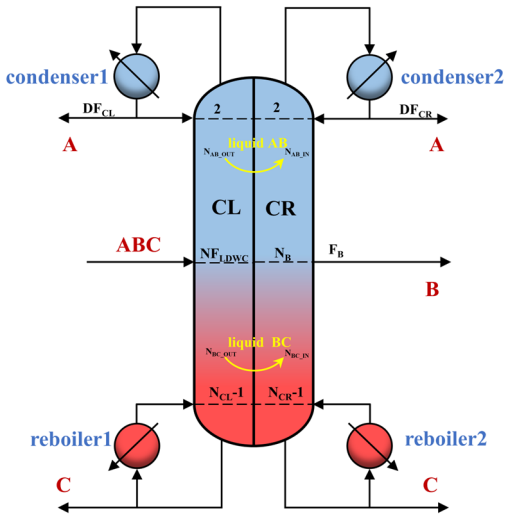

Figure 1. Diagrammatic schematic of LDWC. Where DF_{CL} is the distillate flow rate of CL, DF_{CR} is the distillate flow rate of CR, and F_B is the flow rate of B.

Vapor–liquid equilibrium (VLE) data are the foundation for distillation separation. Our previous work determined VLE data for the system of 1,2-ED and 1,3-PD at 101.3 kPa [17]. The VLE data for the system 1,2-PD + 1,4-BD at 10 kPa, 20 kPa, and 40 kPa have been measured by Yang et al. [18]. However, VLE data for the two binary mixtures 1,2-ED + 1,4-BD and 1,3-PD + 1,4-BD at 101.3 kPa were not found in the NIST Thermodata Engine. Thus, the VLE data for these two binary mixtures at 101.3 kPa are measured and then regressed by activity coefficient models including Wilson [19], NRTL [20], and UNIQUAC [21] via Aspen Plus V11. It is unclear that the performance of the LDWC is used for the diols mixtures separation. Therefore, the LDWC for the diols mixtures separation is simulated using Aspen Plus based on the correlated binary interaction parameters. And DCDS, as illustrated in Figure 2, is carried out as the base case. For a fair comparison, sequential iterative optimization procedures were used to minimize the total annual cost of each configuration. This study can promote the industrial application of LDWC for diols separation.

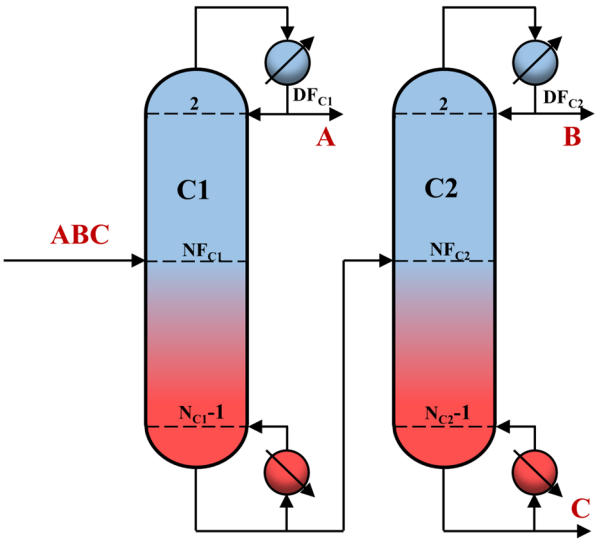

Figure 2. Diagrammatic schematic of DCDS. Where DF_{C1} is the distillate flow rate of C1, DF_{C2} is the distillate flow rate of C2.

2. Experimental and Process Modeling

2.1. Materials

1,2-ED, 1,3-PD, and 1,4-BD were the chemical reagents utilized in this investigation. Their purity is checked by gas chromatography (Zhejiang Fuli Instruments, GC-9790plus, Taizhou, China). The detailed information, including density and boiling point, is summarized in Table 1. It is important to note that these chemicals are used without further treatment.

Table 1. Details of chemical reagents [a].

Component	CAS	Supplier	Purity (wt %)	Density (g·cm^{-3})		Boiling Point (K)		Analysis Method
				Exp [c]	Lit [d]	Exp [e]	Lit [f]	
1,2-ED	107-21-1	Sinopharm, Beijing, China	≥99.0	1112	1110 [22]	470.25	470.45 [23]	GC [b]
1,3-PD	504-63-2	Accela, Shanghai, China	≥98.0	1053	1050 [24]	487.35	487.55 [24]	
1,4-BD	110-63-4	Sinopharm, Beijing, China	≥99.0	1012	1016.9 [25]	501.05	501.15 [25]	

[a] Standard uncertainties of T and p are $u(T)$ = 0.1 K and $u(p)$ = 0.1 kPa, respectively. [b] Gas chromatography. [d, f] Reported in literature. [c] Experiments conducted at 293.75 K. [e] Experiments performed at 101.3 kPa.

2.2. Methods

A modified Rose equilibrium still, depicted in Figure 3, was employed to determine VLE data in this study. Our previous work [26,27] demonstrated the reliability of the apparatus. The apparatus facilitates the establishment of equilibrium by continuous recirculation of both the vapor and liquid phases. For each experiment, 40 mL of the liquid mixture was added to the modified Rose still. Then, the heating rate was tuned to maintain a vapor phase condensation rate of approximately 60 drops per minute. After the temperatures of the vapor and liquid phases were maintained for more than 60 min, equilibrium was reached. Then, both liquid and condensed vapor were sampled for subsequent analysis.

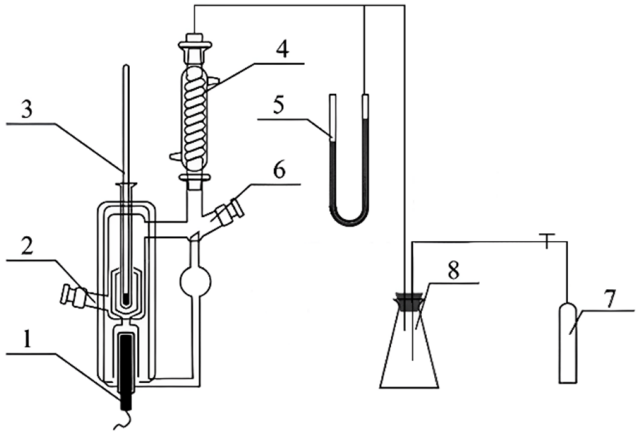

Figure 3. Apparatus for the VLE: (1) electric heating rod; (2) a port for liquid-phase sampling; (3) thermometer; (4) condenser tube; (5) U-shaped mercury differential manometer; (6) a port for vapor-phase sampling; (7) nitrogen cylinder; and (8) buffer vessel.

Two precision mercury thermometers were used to measure the equilibrium temperature. These two thermometers, respectively, have a scale from 150 °C to 200 °C and 200 °C to 250 °C, with a division value of 0.1 °C. Nitrogen was continually added from the nitrogen cylinder to control the pressure. The standard uncertainties of T and p were 0.1 K and 0.1 kPa, respectively. It is noted that the conversion from Celsius to Kelvin is obtained by adding 273.15 and then rounding up.

Gas chromatography (Zhejiang Fuli Instruments, GC-9790plus) with a flame ionization detector (FID) and a capillary column (PEG-20M, 30 m × 0.32 mm × 0.5 μm) was used to examine each sample. A total of 0.1 μL of the sample was injected each time. The carrier gas was high-purity nitrogen (99.999%, wt) at a flow rate of 30 mL/min. Both the detector and the injector had a temperature of 523.15 K. The temperature of the column was programmed in the following manner: initially, it was maintained at a temperature of 373.15 K for a duration of 4 min. Subsequently, the temperature was raised to 503.15 K at a rate of 5 K per minute and held at this temperature for a period of 3 min. To assure accuracy, each sample was measured at least three times.

2.3. Simulation

The simulation employed a mixture consisting of 1,2-ED, 1,3-PD, and 1,4-BD. The feed was introduced at a flow rate of 100 kmol/h, featuring a uniform distribution of mole fractions, representing a challenging separation scenario. All products' target concentration was assumed to be 99.0 mol%. The operational pressure remained consistent with the experimental conditions.

RadFrac module can be used for rigorous calculation for conventional distillation columns. However, no built-in module is available for LDWC in Aspen Plus. When the heat transfer on both sides of the partition is ignored, the equivalent model of LDWC can be derived by the RadFrac modules [15,16], as illustrated in Figure 4.

2.4. Optimization

The simplicity of sequential iterative optimization procedures has contributed to their extensive application in the optimization of diverse distillation systems [28–30]. Therefore, two sequential iterative optimization procedures are proposed to optimize DCDS and LDWC, as illustrated in Figures 5 and 6, respectively. Herein, the primary objective is to minimize the total annual cost (TAC) because it simultaneously considers operating cost and capital cost. TAC in this study can be calculated by the Douglas equations [31], which are provided in Appendix A.

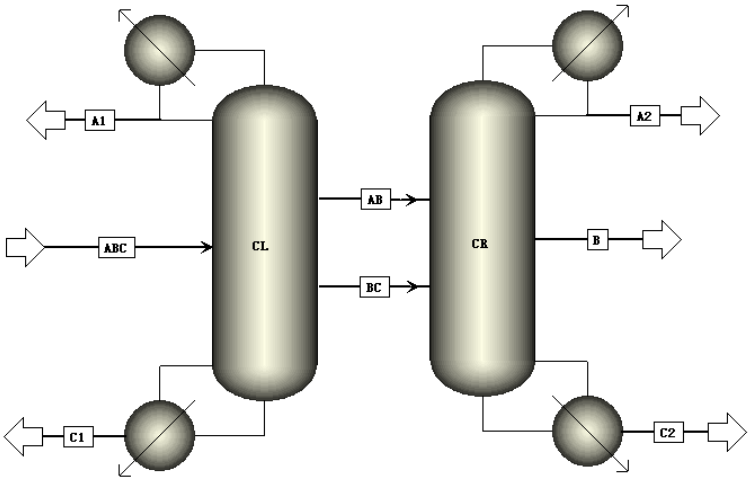

Figure 4. The equivalent model for LDWC in Aspen Plus.

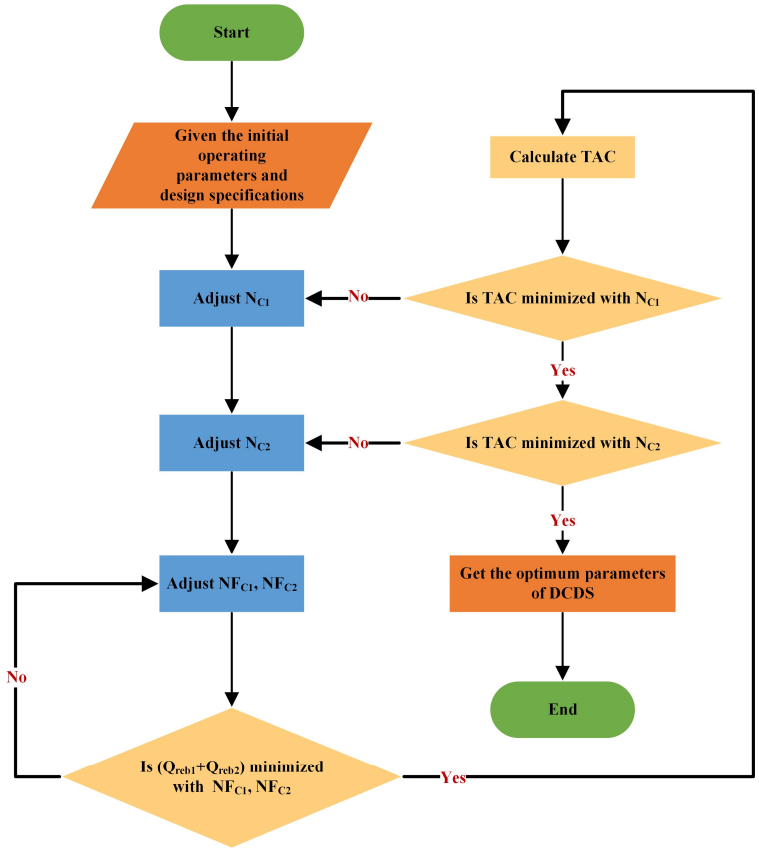

Figure 5. Optimization procedure for DCDS.

As shown in Figure 2, DCDS has four independent discrete design variables and four independent continuous design variables. The discrete design variables include the total theoretical stages of C1 and C2 (N_{C1}, N_{C2}) and the feed stage locations of C1 and C2 (NF_{C1}, NF_{C2}). The continuous design variables include the distillation flow rates of C1 and C2 (DF_{C1}, DF_{C2}) and the reflux ratios of C1 and C2 (RR_{C1}, RR_{C2}). The sequence iterative optimization procedure of DCDS can be manipulated as follows:

(1) Specify the initial operation parameters and use *Design specifications* and *vary* modules in simulation to maintain target purity. Herein, target purity is achieved by manipulating DF_{C1}, DF_{C2}, RR_{C1}, and RR_{C2} using these two modules.
(2) Adjust NF_{C1} and NF_{C2} to minimize the total heat duty (Q_{reb1} + Q_{reb2}).

(3) If the TAC is minimized with N_{C1}, obtain the optimum N_{C1}; if not, adjust N_{C1} and go back to step 2.
(4) If the TAC is minimized with N_{C2}, obtain the optimum N_{C2}; if not, adjust N_{C2} and go back to step 2.
(5) Obtain the optimum parameters of DCDS.

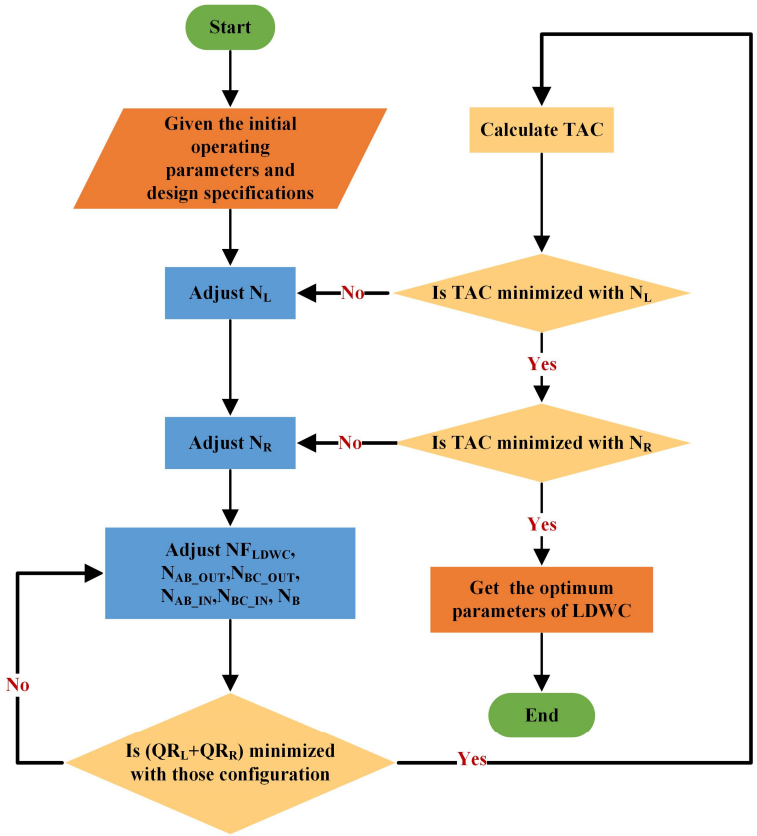

Figure 6. Optimization procedure for LDWC.

LDWC, shown in Figure 1, involved eight independent discrete design variables and seven independent continuous design variables. The eight discrete variables are the total theoretical stages of CL and CR (N_{CL}, N_{CR}), the feed stages location of CL and CR (NF_{LDWC}, N_{AB_IN}, N_{BC_IN}), and the side-draw stages location of CL and CR (N_{AB_OUT}, N_{BC_OUT}, N_B). The seven continuous variables are the distillation flow rates and reflux ratios of CL and CR section (DF_{CL}, DF_{CR}, RR_{CL}, RR_{CR}), the flow rates of liquid-only transfer streams AB and BC(F_{AB}, F_{BC}), and the side-draw stage flow rate (F_B). In the sequence iterative optimization procedure of LDWC, the optimum parameters can be obtained as follows:

(1) Specify the initial operation parameters and use design specifications in Aspen Plus to maintain target purity. Herein, target purity is obtained by manipulating DF_{CL}, DF_{CR}, RR_{CL}, RR_{CR}, and F_B using these two modules.
(2) Adjust NF_{LDWC}, N_{AB_OUT}, N_{BC_OUT}, N_{AB_IN}, N_{BC_IN}, and N_B to minimize the total heat duty (QR_L + QR_R).
(3) If the TAC is minimized with N_L, get the optimum N_L; if not, adjust N_L and go back to step 2.
(4) If the TAC is minimized with N_R, get the optimum N_R; if not, adjust N_R and go back to step 2.
(5) Get the optimum parameters of DCDS.

In addition, the related discrete and continuous design variables for DCDS and LDWC are marked in Figures 1 and 2.

3. Results and Discussion

3.1. Phase Equilibrium Data

The VLE data of 1,2-ED (1) + 1,4-BD (2) and 1,3-PD (1) + 1,4-BD (2) at 101.3 kPa are listed in Appendix B. The vapor and liquid phase equilibrium relationship is expressed as Equation (1).

$$\varphi_i^v p y_i = \gamma_i x_i p_i^s \varphi_i^s \exp\left(\frac{V_i^L (p - p_i^s)}{RT}\right) \quad (1)$$

where T and p are the temperature and pressure of the systems, respectively; x_i and y_i are mole fractions of component i in the liquid and vapor phases, respectively; γ_i is the activity coefficient of component i in the liquid phase; R is the gas constant; and V_i^L is the liquid mole volume of pure component i.

Meanwhile, $\varphi_i{}^v$ and $\varphi_i{}^s$ represent the fugacity coefficient of component i in the vapor and saturated vapor phases, respectively. The vapor phase can be treated as an ideal gas at 101.3 kPa [32], which means that the last term on the right of Equation (1), $\varphi_i{}^v$, and $\varphi_i{}^s$ can be assumed to be 1. Thus, the VLE relationship can be simplified as Equation (2).

$$p y_i = \gamma_i x_i p_i^s \quad (2)$$

where $p_i{}^s$ is the saturated vapor pressure of pure component i. It can be calculated by Extended Antoine Equation (3).

$$\ln(p_i^s) = C_{1i} + \frac{C_{2i}}{T + C_{3i}} + C_{4i} T + C_{5i} \ln(T) + C_{6i} T^{C_{7i}} \text{ for } C_{8i} \le T \le C_{9i} \quad (3)$$

where the constants C_{1i}–C_{9i} are Extended Antoine Coefficients for component i, which are listed in Table 2.

Table 2. Antoine coefficients for vapor pressure [a].

Component	C_{1i}	C_{2i}	C_{3i}	C_{4i}	C_{5i}	C_{6i}	C_{7i}	C_{8i}	C_{9i}
1,2-ED [b]	84.09	10411	0	0	8.1976	1.65×10^{-18}	6	260.15	720
1,3-PD [b]	115.58	−11732	0	0	−13.174	6.55×10^{-6}	2	246.45	724
1,4-BD [b]	105.76	−12811	0	0	−11.069	9.44×10^{-18}	6	293.05	667

[a] from Aspen Plus. [b] T/K, p/Pa.

3.2. Thermodynamic Consistency Test

In this study, both the Redlich–Kister method [33] and the Van Ness method modified by Fredenslund [34] were used to check the thermodynamic consistency of VLE data.

The Redlich–Kister test is expressed as Equation (4).

$$D = 100 \frac{\left| \int_0^1 \ln(\gamma_1/\gamma_2) dx_1 \right|}{\int_0^1 |\ln(\gamma_1/\gamma_2)| dx_1} \le 2 \quad (4)$$

where γ_1 and γ_2 is the activity coefficient of component 1 and 2, respectively; x_1 is the mole fraction of component 1. When the value of D is no greater than 2 [33], the VLE data can be considered thermodynamically consistency. Meanwhile, the Redlich–Kister plots for two binary systems are illustrated in Figure 7.

The Van Ness method modified by Fredenslund, i.e., the Fredenslund test, is expressed as Equation (5).

$$\Delta y = \frac{1}{N} \sum_{i=1}^{N} \left| y_i^{\exp} - y_i^{cal} \right| \le 0.01 \quad (5)$$

where N represents the number of experimental data points, $y^{\exp}$ is the experimental data of y, and y^{cal} is the calculated value. According to this method, the value of Δy should not be more than 0.01 for thermodynamic consistency [34].

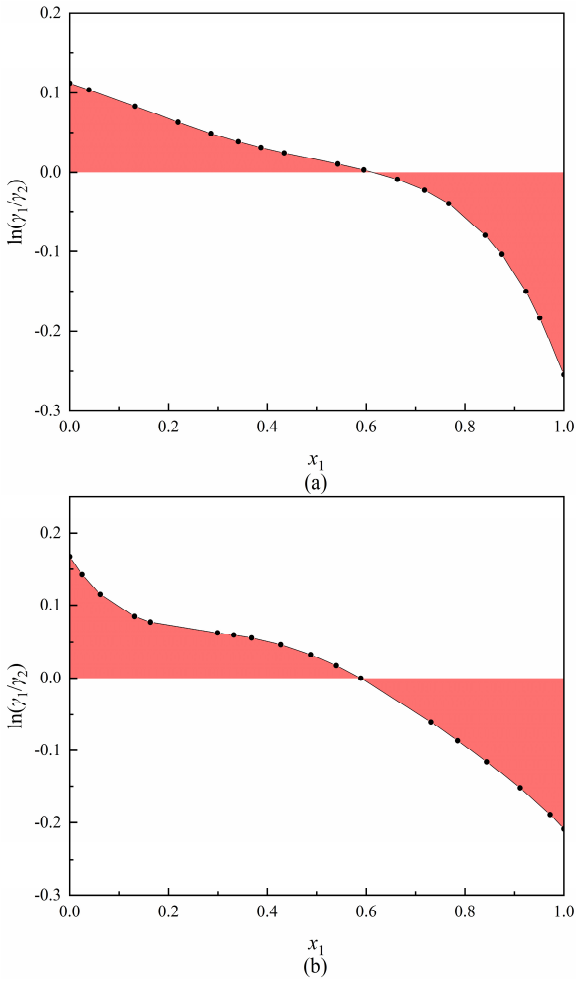

Figure 7. Redlich–Kister plots for the binary system of (**a**) 1,2-ED (1) + 1,4-BD (2), (**b**) 1,3-PD (1) + 1,4-BD (2).

Nevertheless, it should be noted that the Fredenslund test alone may not provide a comprehensive evaluation of thermodynamic consistency [35], as it does not consider potential local inconsistencies. Therefore, the residual disturbances of equilibrium temperature and vapor composition, as depicted in Figures 8 and 9, should be analyzed. They were calculated from Equations (6) and (7) [36]. According to the distribution results in the figures, the data has local consistency.

$$\Delta T = T_{\text{exp}} - T_{\text{cal}} \tag{6}$$

$$\Delta y = y_{\text{exp}} - y_{\text{cal}} \tag{7}$$

The results of the Redlich–Kister test and the Fredenslund test are listed in Table 3. The values of D for 1,2-ED (1) + 1,4-BD (2) and 1,3-PD (1) + 1,4-BD (2) are 0.9078 and 0.9321, respectively. They are both less than 2. Meanwhile, the Δy values are 0.0026 and 0.0018, respectively. They are both less than 0.01. Thus, the experimental VLE data for these two binary systems exhibit thermodynamic consistency.

Table 3. The thermodynamic consistency test results.

System	D	Δy_1 [a]
1,2-ED (1)—1,4-BD (2)	1.77	0.0014
1,3-PD (1)—1,4-BD (2)	0.22	0.0008

[a] Testified by the NRTL model.

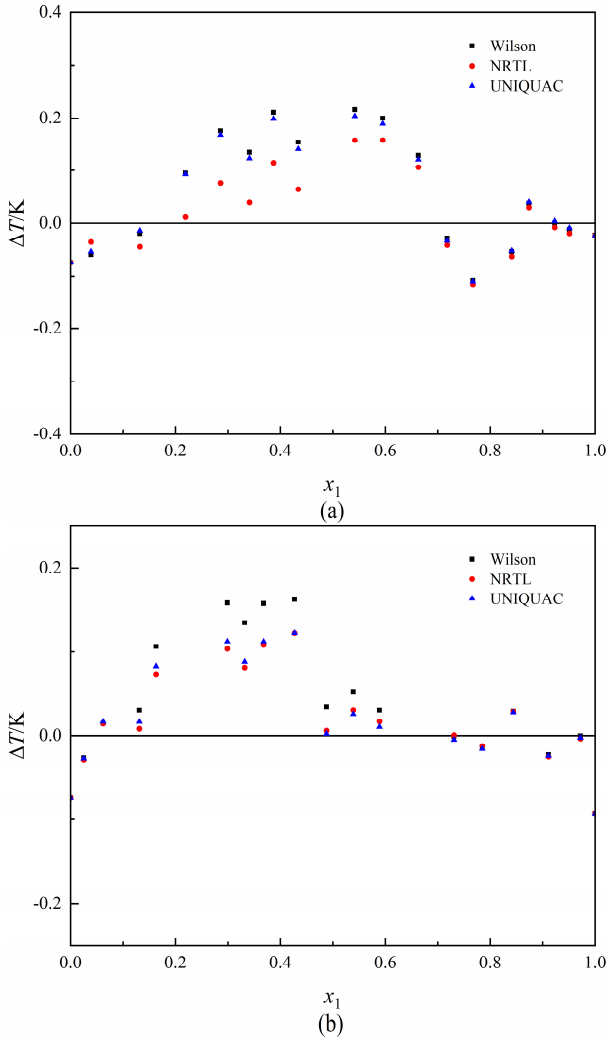

Figure 8. Residual disturbance for the equilibrium temperature (T) with liquid composition (x_1) of (**a**) 1,2-ED (1) + 1,4-BD (2), (**b**) 1,3-PD (1) + 1,4-BD (2).

3.3. Data Regression

In this study, the Wilson, NRTL, and UNIQUAC activity coefficient models were used to regress the VLE data. These models can be found in Aspen Plus and listed in Appendix C. The maximum likelihood objective function was taken to regress the binary interaction parameters and expressed as Equation (8).

$$Q = \sum_{i=1}^{N} \left[\left(\frac{p_i^{\exp} - p_i^{\text{cal}}}{\sigma_p} \right)^2 + \left(\frac{T_i^{\exp} - T_i^{\text{cal}}}{\sigma_T} \right)^2 + \left(\frac{x_{1,i}^{\exp} - x_{1,i}^{\text{cal}}}{\sigma_x} \right)^2 + \left(\frac{y_{1,i}^{\exp} - y_{1,i}^{\text{cal}}}{\sigma_y} \right)^2 \right] \quad (8)$$

where N is the number of experimental data, σ_T, σ_P, σ_x, and σ_y represent the standard deviations of T, p, x, and y, respectively. The nonrandom interaction parameter (α_{ij}) was set as 0.3 in the NRTL model. Table 4 summarizes all the regressed binary interaction parameters.

Additionally, the root mean square deviation (RMSD) and average absolute deviation (AAD) were computed. When comparing experimental data with the calculated values, RMSD assesses how dispersed the data are, while ADD assesses how closely they coincide with each other.

As shown in Table 5, the AAD of T is no more than 0.10 and 0.06, while the AAD of y_1 is no more than 0.0018 and 0.0009 for the two binary systems, respectively. RMSD of T is no more than 0.12 and 0.08, while RMSD of y_1 is no more than 0.0030 and 0.0012, respectively.

Consequently, the VLE data can be effectively correlated using the three models. NRTL is taken for the following study because it presents the least AAD and RMSD for these two binary systems.

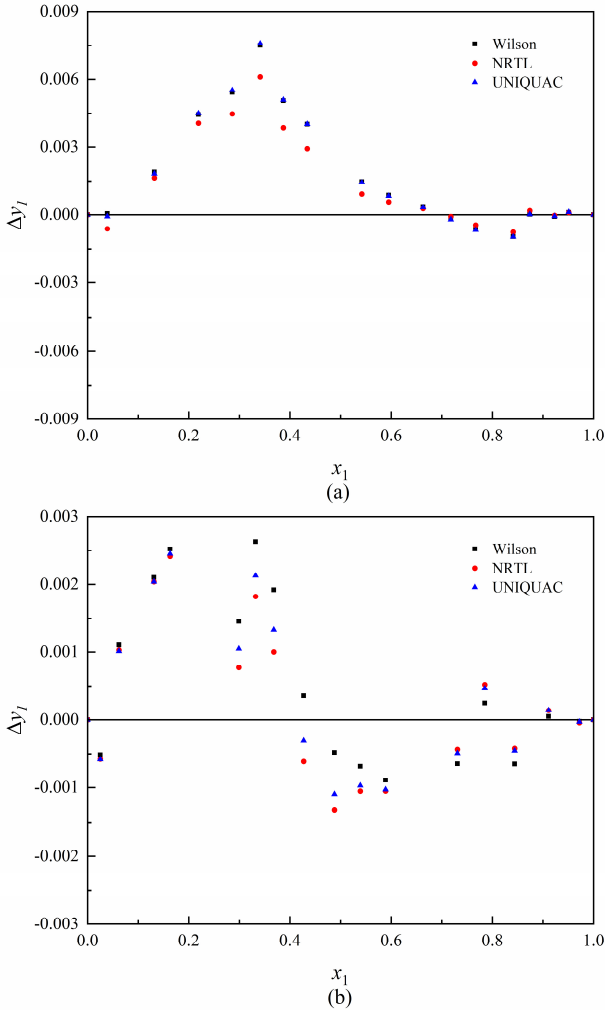

Figure 9. Residual disturbance for vapor composition (y_1) with liquid composition (x_1) of (**a**) 1,2-ED (1) + 1,4-BD (2), (**b**) 1,3-PD (1) + 1,4-BD (2).

Table 4. Correlated parameters of Wilson, NRTL, and UNIQUAC for 1,2-ED (1) + 1,4-BD (2) and 1,3-PD (1) + 1,4-BD (2).

Model	a_{12}	a_{21}	b_{12}	b_{21}	α
1,2-ED (1) + 1,4-BD (2)					
Wilson	1.54	−5.40	−479.79	2111.72	-
NRTL	−19.57	12.58	9926.34	6373.18	0.3
UNIQUAC	−3.57	2.00	1497.94	−823.53	-
1,3-PD (1) + 1,4-BD (2)					
Wilson	4.50	−8.26	−2057.22	3767.51	-
NRTL	−30.09	22.47	15,144.8	−11,261.3	0.3
UNIQUAC	11.57	−9.60	−5820.44	4809.73	-
1,2-ED (1) + 1,3-PD (2) [α]					
Wilson	−141.12	91.50	0	0	-
NRTL	−14.78	50.33	0	0	0.3
UNIQUAC	116.52	−154.33	0	0	-

[α] Binary interaction parameters used in simulation come from our previous work [17].

Table 5. AAD and RMSD for 1,2-ED (1) + 1,4-BD (2), and 1,3-PD (1) + 1,4-BD (2).

Model	AAD (T) [a]	AAD (y_1) [a]	RMSD (T) [b]	RMSD (y_1) [b]
1,2-ED (1) + 1,4-BD (2)				
Wilson	0.10	0.0018	0.12	0.0029
NRTL	0.07	0.0014	0.08	0.0024
UNIQUAC	0.09	0.0018	0.11	0.0030
1,3-PD (1) + 1,4-BD (2)				
Wilson	0.06	0.0009	0.08	0.0012
NRTL	0.05	0.0008	0.06	0.0011
UNIQUAC	0.05	0.0008	0.06	0.0011

[a] AAD = $\frac{\sum_{i=1}^{N}\left|\theta_{i,exp}-\theta_{i,cal}\right|}{N}$, [b] RMSD = $\left(\sum_{i=1}^{N}\frac{\left(\theta_{i,exp}-\theta_{i,cal}\right)^2}{N}\right)^{0.5}$. where N is the number of experimental data points, θ is the parameter (T and y in this study).

The T–x–y diagrams for experimental data and correlated data using the Wilson, NRTL, and UNIQUAC models for 1,2-EG (1) + 1,4-BD (2) and 1,3-PD (1) + 1,4-BD (2) are shown in Figure 10.

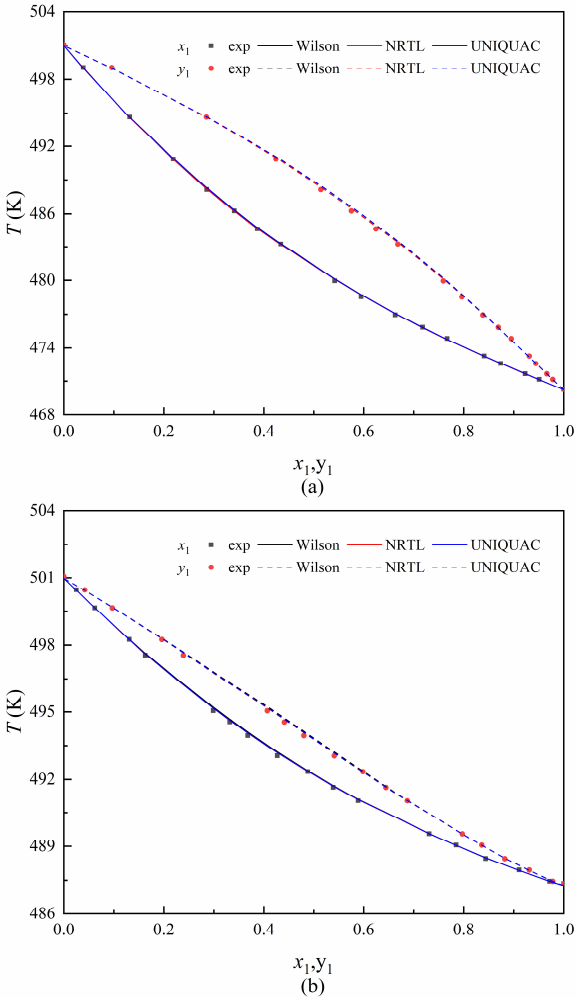

Figure 10. T–x–y diagram for (**a**) 1,2-EG (1) + 1,4-BD (2) and (**b**) 1,3-PD (1) + 1,4-BD (2) at 101.3 kPa using Wilson, NRTL, and UNIQUAC models.

Meanwhile, the activity coefficient of experimental data and values calculated by the Wilson, NRTL, and UNIQUAC models for the two binary systems are shown in Figures 11 and 12, respectively. These Figures show that the activity coefficient varies monotonically with liquid phase composition.

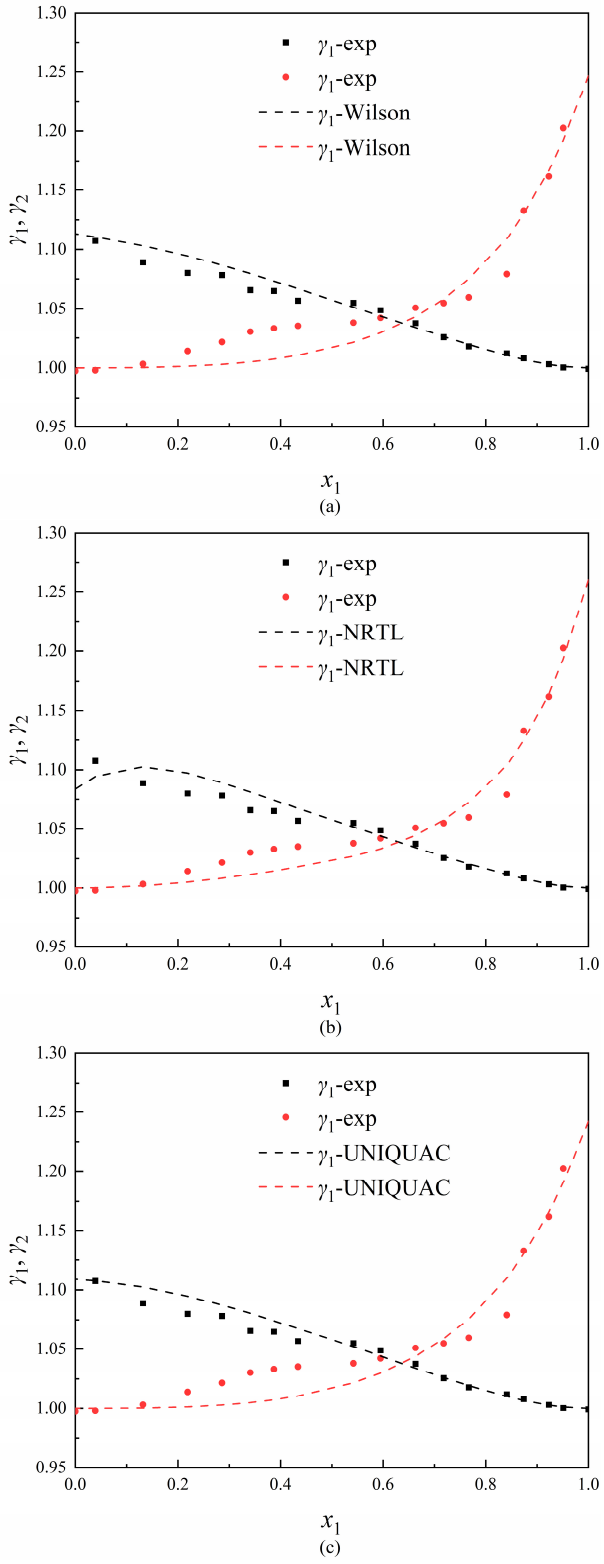

Figure 11. The activity coefficient for experimental and correlated data for 1,2-EG (1) + 1,4-BD (2) using (**a**) Wilson, (**b**) NRTL, and (**c**) UNIQUAC models.

3.4. Optimization Results and Comparison

For DCDS, the optimization process can be found in Figure 13, which shows the relationship between TAC and the stages of C1 (NC1) and C2 (NC2). The TAC presents an initial rapid decrease with the increase of the two columns' stages, followed by a gradual

increase. The minimum TAC of 2,213,017 $/year for DCDS is achieved when N_{C1} and N_{C2} are 62 and 58, respectively. The optimization process for LDWC is illustrated in Figure 14, which displays the relationship between the stage in the left column CL (N_L) or right column CR (N_R) and TAC. The TAC first rapidly decreases, then slowly increases with the increasing N_L, while it rapidly decreases and then quickly increases with increasing N_R. The minimum TAC of 1,839,766 $/year for LDWC is obtained while the N_L is set as 92 and the N_R is 116.

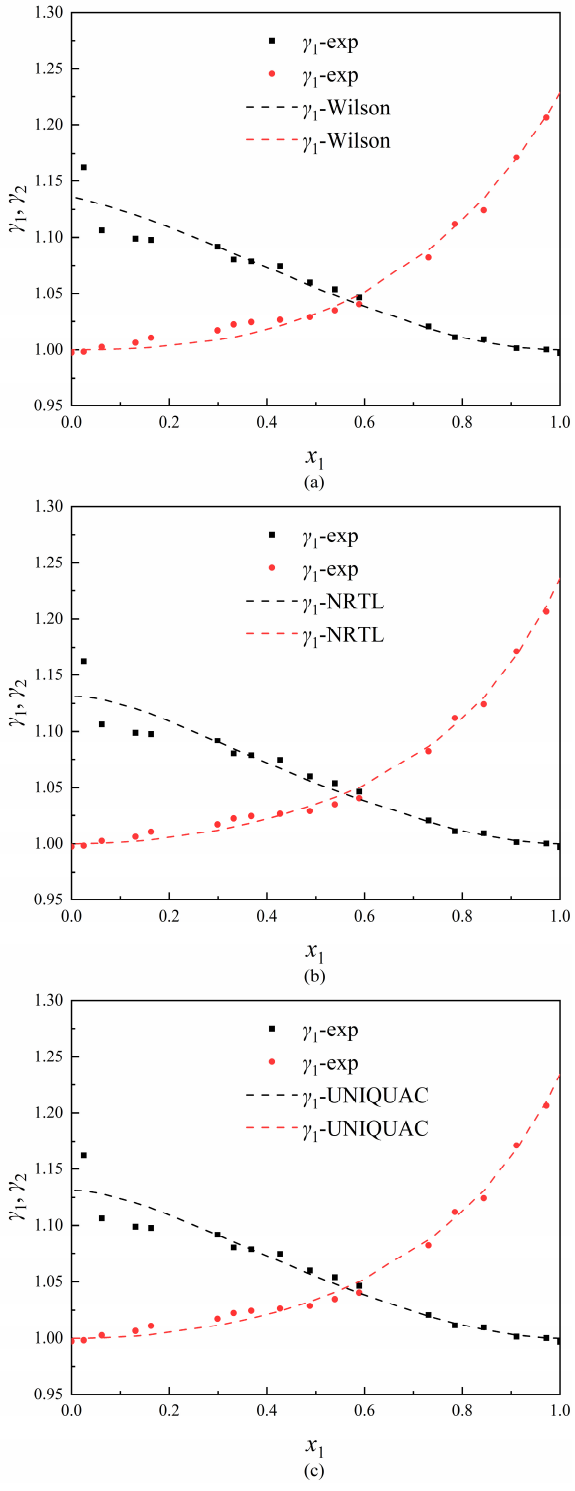

Figure 12. The activity coefficient for experimental and correlated data for 1,3-PD (1) + 1,4-BD (2) using (**a**) Wilson, (**b**) NRTL, and (**c**) UNIQUAC models.

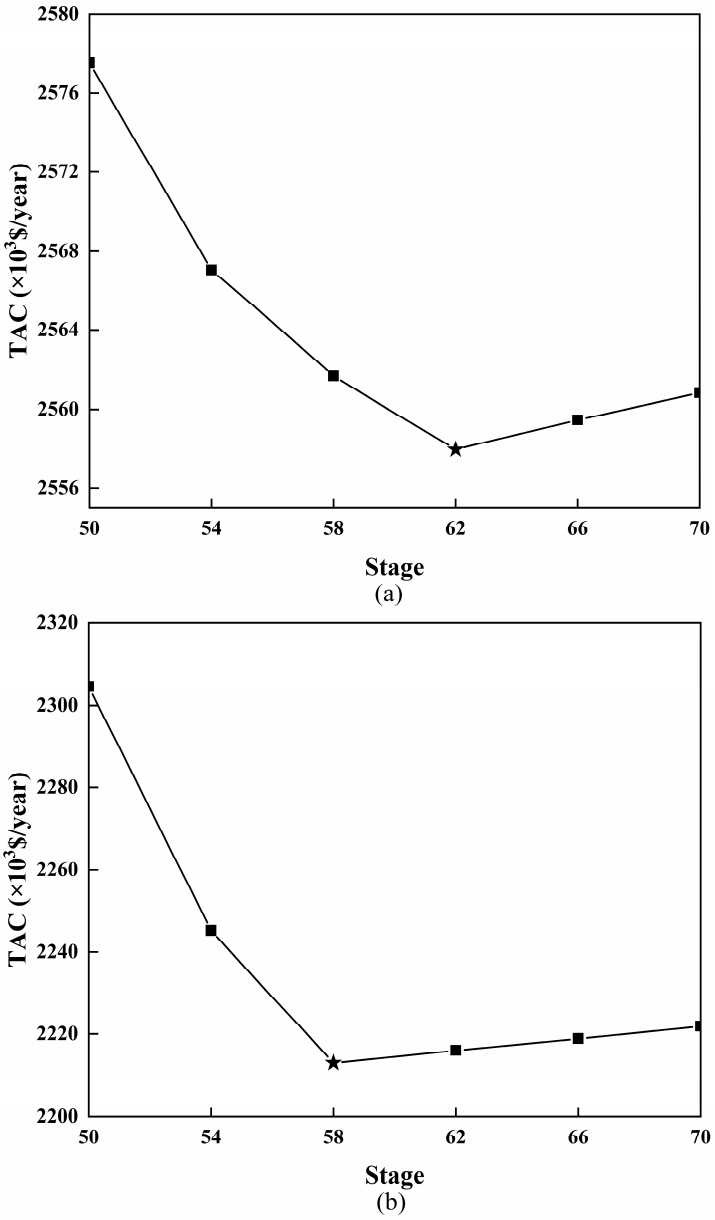

Figure 13. The relationship between TAC and stages of (**a**) C1 and (**b**) C2 for DCDS.

The detailed costs for the optimized DCDS and LDWC are listed in Table 6. Despite LDWC incurring a higher capital cost of 7.39% compared with DCDS, it involves a lower operating cost of 19.31% due to the lower energy requirement. As a result, TAC for LDWC can be reduced by 16.8% compared with DCDS.

The optimum design parameters for DCDS and LDWC are displayed in Figure 15, where 1,2-ED, 1,3-PD, and 1,4-BD are marked as A, B, and C, respectively. Figure 15a shows that the reboilers' duties of DCDS are 4005 kW and 3234 kW, while the condensers' duties of DCDS are 1697 kW and 3205 kW, respectively. From Figure 15b, the reboilers' duties of LDWC are 3665 kW and 2181 kW, and the condensers' duties of LDWC are 1356 kW and 2154 kW, respectively. As a result, LDWC achieves energy savings of 19.24% for heating utility and 28.40% for cooling utility than DCDS.

Table 6. Detailed cost of DCDS and LDWC.

	DCDS	LDWC
Capital cost ($)	2,028,300	2,178,246
Shell	1,196,753	1,409,168
Tray	89,091	128,568
Heat exchanger	742,456	640,510
CC Saving (%)	0	−7.39
Operating cost ($/year)	2,010,187	1,621,942
Heating utilities	1,936,378	1,586,162
Cooling utilities	73,809	35,779
OC Saving (%)	0	19.31
TAC * ($/year)	2,213,017	1,839,766
TAC Saving (%)	0	16.87

* The payback year was assumed at 10.

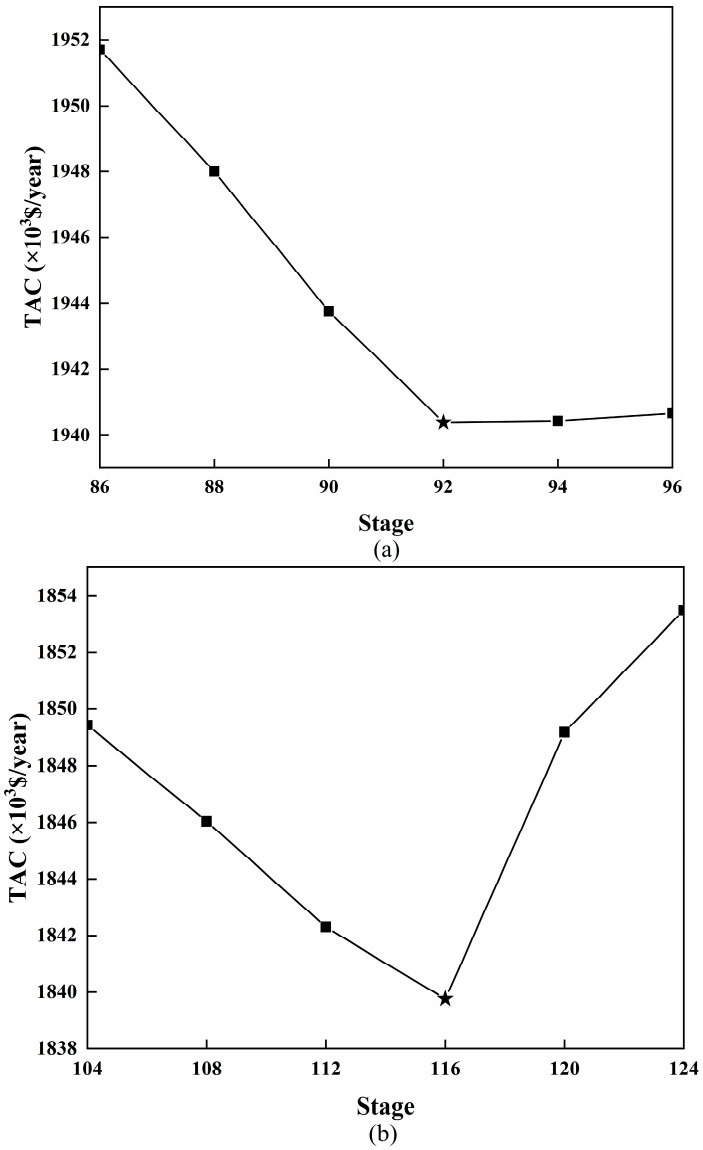

Figure 14. The relationship between TAC and stages of (**a**) CL and (**b**) CR for LDWC.

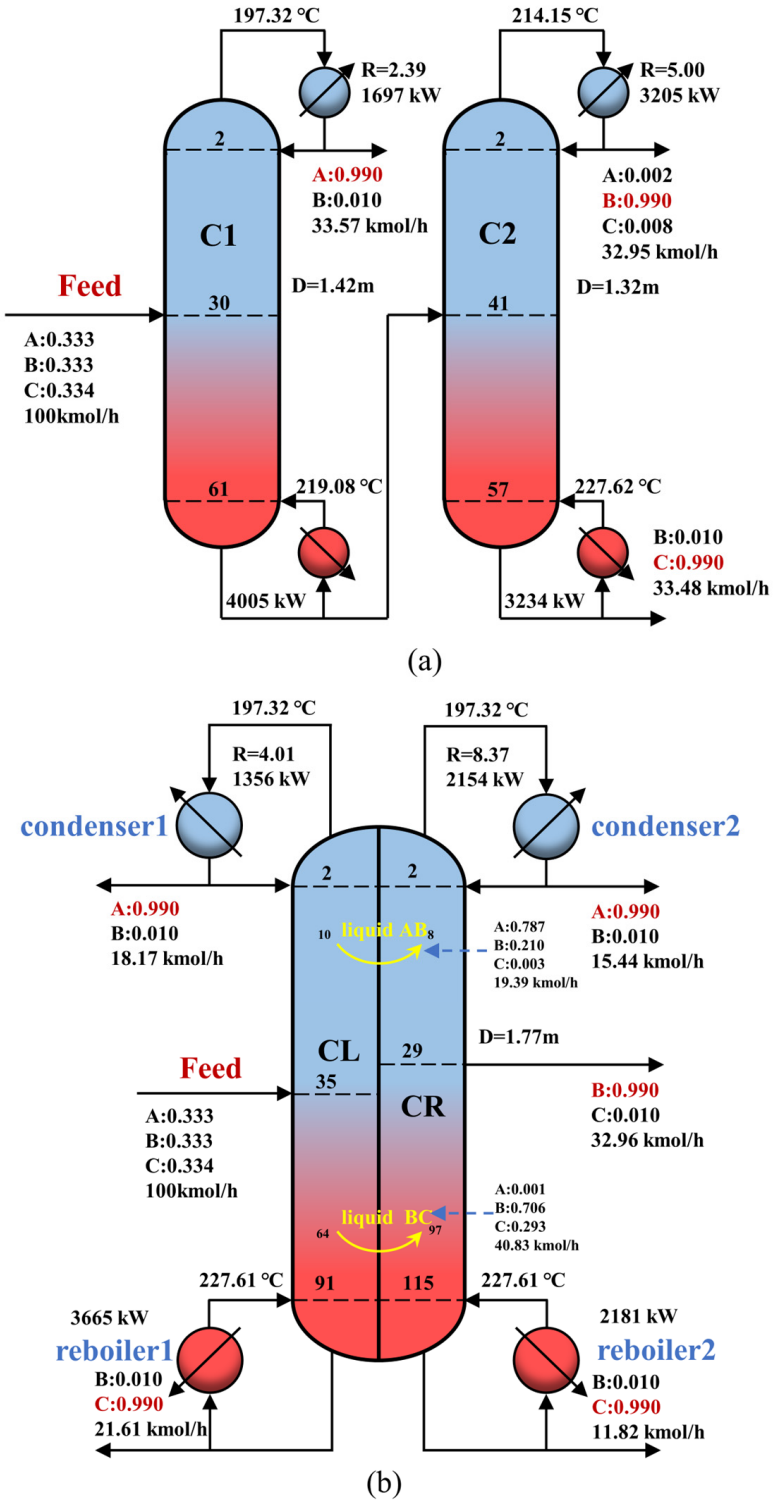

Figure 15. Simulation results of (**a**) DCDS and (**b**) LDWC.

Figure 16 illustrates the liquid composition of C1 and C2 in DCDS. The concentrations of 1,2-ED and 1,4-ED exhibit a consistent monotonic change along the columns. However, the concentration of 1,3-PD within C1 presents two distinct peaks in the rectifying and stripping section, which requires additional energy to satisfy product specifications. As illustrated in Figure 17, 1,3-PD is withdrawn in the highest concentration zone for LDWC, which is similar to the DWC for ternary mixture separation and reduces the re-mixing of the middle component. Thus, LDWC has a lower energy consumption compared to DCDS.

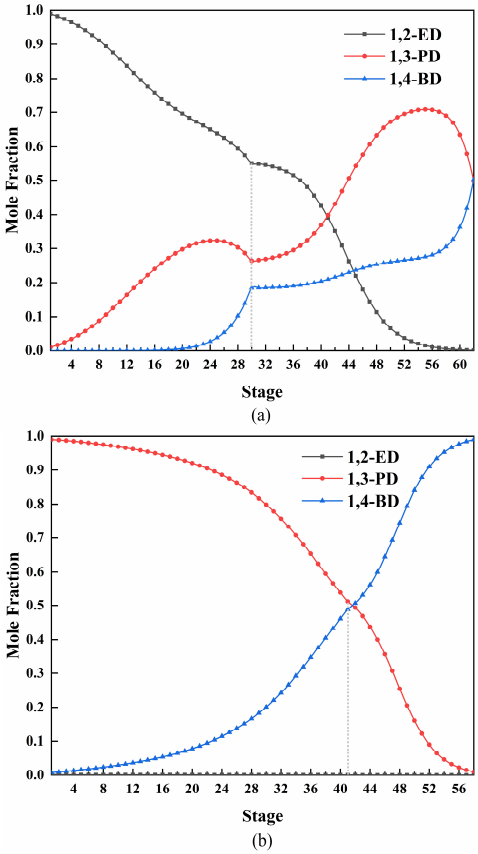

Figure 16. Liquid composition profiles of (**a**) C1, (**b**) C2 in DCDS.

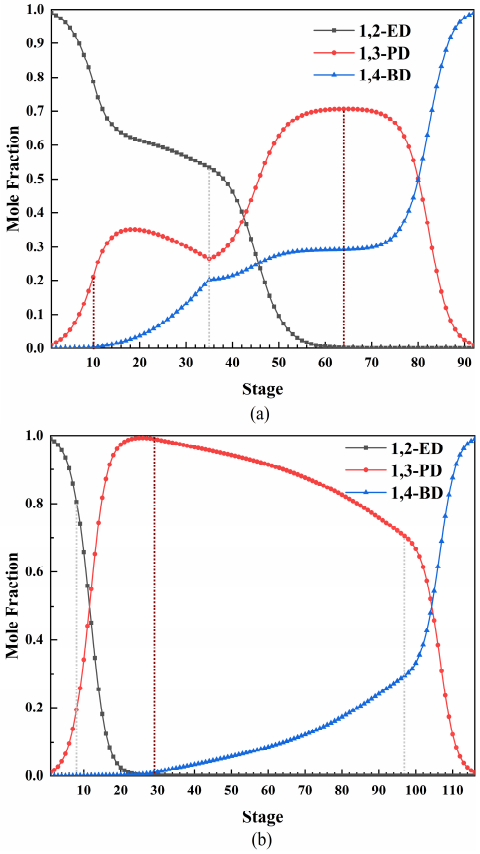

Figure 17. Liquid profiles of (**a**) CL and (**b**) CR in LDWC.

4. Conclusions

In this study, we determine the VLE data for the binary systems of 1,2-ED + 1,4-BD and 1,3-PD + 1,4-BD at 101.3 kPa. Redlich–Kister and Fredenslund tests are employed to validate the reliability of measured data. The Redlich–Kister test parameter D is less than 2, and the Fredenslund test parameter Δy is less than 0.01, demonstrating that the VLE data present thermodynamic consistency. Additionally, VLE data are regressed using the Wilson, NRTL, and UNIQUAC activity coefficient models. AAD(T) and AAD(y_1) are no more than 0.10 K and 0.0018, respectively, and RMSD(T) and RMSD(y_1) are no more than 0.12 K and 0.0030, respectively, which indicate that the VLE data can be correlated well with all three models. Based on regression binary interaction parameters, DCDS and LDWC are designed and optimized for separating a ternary mixture including 1,2-ED, 1,3-PD, and 1,4-BD by the NRTL model. As a result, LDWC can reduce TAC by 16.87% and cooling and heating utility consumptions by 28.40% and 19.24%, respectively, compared with DCDS.

Author Contributions: Conceptualization, Y.-Y.W. and Z.-W.S.; methodology, Z.-W.S. and J.-B.R.; software, Z.-W.S. and J.-B.R.; validation, Y.-X.Y.; formal analysis, B.W.; investigation, Z.-W.S.; resources, J.-B.R.; data curation, K.C. and L.-J.J.; writing—original draft preparation, Z.-W.S.; writing—review and editing, Y.-Y.W.; visualization, Z.-W.S.; supervision, Y.-X.Y.; project administration, Y.-Y.W. All authors have read and agreed to the published version of the manuscript.

Funding: This research received no external funding.

Data Availability Statement: No new data were created.

Conflicts of Interest: The authors declare no conflict of interest.

Appendix A. TAC Estimation

TAC was defined as follows [31]:

$$TAC\ (\$/year) = Operating\ Cost + \frac{Capital\ Cost}{Payback\ Year} \tag{A1}$$

The capital cost (CC) is determined by the aggregate installed cost, which encompasses the expenditure associated with procuring and installing the principal equipment [37]. The principal equipment consists of heat exchangers, trays, and column shells. In this discussion, operating cost (OC) refers to the aggregate expenditure incurred for cooling and heating utilities. The payback time for this study has been assumed to be 10 years [38], with an annual operational duration of 8000 h. Furthermore, it is estimated that the cost of cooling water is 0.354 \$/GJ [39]. The cost of steam with high pressure can be estimated using data obtained from the TLV platform [40], as outlined in Table A1.

Table A1. The cost associated with high-pressure steam.

Steam Pressure (BarG)	Latent Heat of Vaporization (kJ/kg)	Price (\$/GJ)	Temperature (K)
40	1705.71	9.18	525
46	1661.15	9.42	533

The installed cost for primary equipment is calculated from the Douglas equations, Equations (A2)–(A6) [31]. The Marshall and Swift index (M & S) is utilized with a value of 1638.2 [41]. It is presumed that all equipment is manufactured using carbon steel.

$$Capital\ cost\ for\ column\ shell\ (\$) = \frac{M\&S}{280} \times 937.636 \times D^{1.066} \times H_c^{0.802} \times (2.18 + F_c) \times \theta \tag{A2}$$

with

$$H_c(m) = (N_{actual} - 1) \times 0.6096 + 6 \tag{A3}$$

where D (m) denotes the diameter of column for DCDS or the equivalent diameter for LDWC, obtainable from the *column internals* in Aspen Plus; F_c denotes the factors, calculated as material factor (F_m) multiplied by pressure factor (F_p); In the case of carbon steel, F_m and F_p have a value of 1; H_c stands for the height of column installation; N_{actual} is the a of actual trays; the penalty factor θ is set at 1 for DCDS and 1.1 for LDWC [42].

$$Capital\ cost\ for\ tray\ (\$) = \frac{M\&S}{280} \times 97.243 \times D^{1.55} \times H_t \times F_c \quad (A4)$$

where F_c stands for the related factor of tray, which can be calculated by the sum of material factor (F_m), type factor (F_t), and tray space factor (F_s); $F_m = 0$, $F_t = 0$, and $F_s = 1$ in carbon steel sieve tray column; H_t denotes the column's stack height, equal to H_c minus 6 m.

$$Capital\ cost\ for\ heat\ exchanger\ (\$) = \frac{M\&S}{280} \times 474.668 \times A^{0.65} \times (2.29 + F_c) \quad (A5)$$

with

$$A(\mathrm{m}^2) = \frac{Q}{U \bullet \Delta T} \quad (A6)$$

where F_c denotes the related factor of the heat exchanger, equal to the product of material factor (F_m) and the sum of type factor (F_t) and pressure factor (F_p); $F_t = 1.35$, $F_p = 0$, and $F_m = 1$ for the shell-tube heat exchanger made of carbon steel in this study; A (m^2) represents the heat exchangers' area; Q (kW) denotes the heating and cooling heat duty; U ($\mathrm{kW/(K \cdot m^2)}$) stands for the coefficient of heat transfer, which is 0.568 in the reboiler and 0.852 in the condenser [43]; ΔT (K) denotes the driving force of temperature [41].

The heating and cooling utilities cost can be calculated from Equations (A7) and (A8).

$$Cooling\ utilities\ cost\ (\$/year) = C_c \times Q_C \times 8000 \quad (A7)$$

$$Heating\ utilities\ cost\ (\$/year) = C_h \times Q_R \times 8000 \quad (A8)$$

where Q_R (GJ/h) and Q_C (GJ/h) represent the heat duty of the reboiler and condenser, respectively; C_h (\$/GJ) and C_c (\$/GJ) are the unit cost of heating and cooling utilities, respectively.

Appendix B. Experimental VLE Data

Table A2. 1,2-ED (1) + 1,4-BD (2) experimental VLE data at 101.3 kPa [a].

T/K	x_1	y_1	${\gamma_1}^{exp}$	${\gamma_2}^{exp}$
470.3	1.000	1.000	0.999	
471.2	0.951	0.978	1.000	1.202
471.7	0.923	0.966	1.003	1.162
472.6	0.874	0.944	1.008	1.133
473.3	0.841	0.931	1.012	1.079
474.9	0.767	0.895	1.018	1.060
475.9	0.718	0.869	1.026	1.055
477.0	0.663	0.838	1.038	1.051
478.6	0.595	0.796	1.049	1.042
480.0	0.542	0.759	1.055	1.038
483.3	0.434	0.668	1.057	1.035
484.7	0.387	0.624	1.065	1.033
486.3	0.341	0.575	1.066	1.030
488.2	0.286	0.514	1.078	1.022
490.9	0.219	0.424	1.080	1.014
494.7	0.132	0.285	1.089	1.003
499.1	0.039	0.096	1.107	0.998
501.1	0.000	0.000		0.997

[a] Standard uncertainties: $u(T) = 0.1$ K, $u(p) = 0.1$ kPa, $u(x) = 0.005$, $u(y) = 0.005$.

Table A3. 1,3-PD (1) + 1,4-BD (2) experimental VLE data at 101.3 kPa [a].

T/K	x_1	y_1	γ_1^{exp}	γ_2^{exp}
487.4	1.000	1.000	0.997	
487.5	0.972	0.978	1.000	1.207
488.0	0.911	0.931	1.002	1.171
488.5	0.844	0.882	1.010	1.124
489.1	0.785	0.836	1.011	1.112
489.6	0.731	0.797	1.021	1.082
491.1	0.589	0.687	1.047	1.040
491.7	0.539	0.644	1.054	1.035
492.4	0.488	0.598	1.060	1.029
493.1	0.427	0.541	1.075	1.026
494.0	0.368	0.48	1.079	1.025
494.6	0.332	0.441	1.080	1.022
495.1	0.299	0.407	1.092	1.017
497.6	0.163	0.239	1.098	1.011
498.3	0.131	0.196	1.099	1.006
499.7	0.062	0.097	1.106	1.003
500.5	0.025	0.042	1.162	0.998
501.1	0.000	0.000		0.997

[a] standard uncertainties: $u(T) = 0.1$ K, $u(p) = 0.1$ kPa, $u(x) = 0.005$, $u(y) = 0.005$.

Appendix C. Activity Coefficient Models

Wilson model

When using the Wilson model, the activity coefficient was calculated as follows:

$$\ln \gamma_i = 1 - \ln\left(\sum_j \Lambda_{ij} x_j\right) - \sum_j \frac{\Lambda_{ji} x_j}{\sum_k \Lambda_{jk} x_k} \tag{A9}$$

$$\ln \Lambda_{ij} = a_{ij} + \frac{b_{ij}}{T} \tag{A10}$$

NRTL model

When using the NRTL model, the activity coefficient was calculated as follows:

$$\ln \gamma_i = \frac{\sum_j x_j \tau_{ji} G_{ji}}{\sum_k x_k G_{ki}} + \sum_j \frac{x_j G_{ij}}{\sum_k x_k G_{ki}} \left(\tau_{ij} - \frac{\sum_m x_m \tau_{mi} G_{mi}}{\sum_k x_k G_{ki}}\right) \tag{A11}$$

$$G_{ij} = \exp\left(-\alpha \tau_{ij}\right) \tag{A12}$$

$$\tau_{ij} = a_{ij} + \frac{b_{ij}}{T} \tag{A13}$$

UNIQUAC model

When using the UNIQUAC model, the activity coefficient was calculated as follows:

$$\ln \gamma_i = \ln \frac{\phi_i}{x_i} + \frac{z}{2} q_i \ln \frac{\theta_i}{\phi_i} - q_i' \ln t_i' - q_i' \sum_j \frac{\theta_i' \tau_{ij}}{t_i'} + l_i + q_i' - \frac{\phi_i}{x_i} \sum_j x_i l_i \tag{A14}$$

$$\theta_i = \frac{\mathrm{q}_i x_i}{\sum_k \mathrm{q}_k x_k} \tag{A15}$$

$$\theta_i' = \frac{q_i' x_i}{\sum_k q_i' x_k} \tag{A16}$$

$$\phi_i = \frac{\mathrm{r}_i x_i}{\sum_k \mathrm{r}_k x_k} \tag{A17}$$

$$l_i = \frac{z}{2}(r_i - q_i) + 1 - r_i \tag{A18}$$

$$t'_i = \sum_k \theta'_k \tau_{ki} \tag{A19}$$

$$\ln \tau_{ij} = a_{ij} + \frac{b_{ij}}{T} \tag{A20}$$

$z = 10$; $q_i = q'_i = 2.248$ (1,2-ED), 2.788 (1,3-PD), and 3.328 (1,4-BD); $r_i = 2.409$ (1,2-ED), 3.083 (1,3-PD), and 3.757 (1,4-BD).

References

1. Liu, Y.; Wang, W.; Zeng, A.-P. Biosynthesizing structurally diverse diols via a general route combining oxidative and reductive formations of OH-groups. *Nat. Commun.* **2022**, *13*, 1595. [CrossRef] [PubMed]
2. Tronconi, E.; Ferlazzo, N.; Forzatti, P.; Pasquon, I.; Casale, B. A mathematical model for the catalytic hydrogenolysis of carbohydrates. *Chem. Eng. Sci.* **1992**, *47*, 2451–2456. [CrossRef]
3. Sholl, D.S.; Lively, R.P. Seven chemical separations to change the world. *Nature* **2016**, *532*, 435–437. [CrossRef] [PubMed]
4. Qian, X.; Liu, R.; Huang, K.; Chen, H.; Yuan, Y.; Zhang, L.; Wang, S. Comparison of Temperature Control and Temperature Difference Control for a Kaibel Dividing Wall Column. *Processes* **2019**, *7*, 773. [CrossRef]
5. Qian, X.; Liu, R.; Huang, K.; Chen, H.; Yuan, Y.; Zhang, L.; Wang, S. Controllability Comparison of the Four-Product Petlyuk Dividing Wall Distillation Column Using Temperature Control Schemes. *Processes* **2020**, *8*, 116. [CrossRef]
6. Rangaiah, G.P.; Feng, Z.; Hoadley, A.F. Multi-Objective Optimization Applications in Chemical Process Engineering: Tutorial and Review. *Processes* **2020**, *8*, 508. [CrossRef]
7. Ye, Q.; Wang, Y.; Pan, H.; Zhou, W.; Yuan, P. Design and Control of Extractive Dividing Wall Column for Separating Dipropyl Ether/1-Propyl Alcohol Mixture. *Processes* **2022**, *10*, 665. [CrossRef]
8. Kaibel, G. Distillation columns with vertical partitions. *Chem. Eng. Technol.* **1987**, *10*, 92–98. [CrossRef]
9. Dejanović, I.; Matijašević, L.; Halvorsen, I.J.; Skogestad, S.; Jansen, H.; Kaibel, B.; Olujić, Ž. Designing four-product dividing wall columns for separation of a multicomponent aromatics mixture. *Chem. Eng. Res. Des.* **2011**, *89*, 1155–1167. [CrossRef]
10. Kolbe, B.; Wenzel, S. Novel distillation concepts using one-shell columns. *Chem. Eng. Process. Process Intensif.* **2004**, *43*, 339–346. [CrossRef]
11. Ling, H.; Luyben, W.L. Temperature Control of the BTX Divided-Wall Column. *Ind. Eng. Chem. Res.* **2010**, *49*, 189–203. [CrossRef]
12. Si, Z.; Chen, H.; Cong, H.; Li, X. Energy, exergy, economic and environmental analysis of a novel steam-driven vapor recompression and organic Rankine cycle intensified dividing wall column. *Sep. Purif. Technol.* **2022**, *295*, 121285. [CrossRef]
13. Ramapriya, G.M.; Tawarmalani, M.; Agrawal, R. Thermal coupling links to liquid-only transfer streams: A path for new dividing wall columns. *AIChE J.* **2014**, *60*, 2949–2961. [CrossRef]
14. Cui, C.; Zhang, X.; Sun, J. Design and optimization of energy-efficient liquid-only side-stream distillation configurations using a stochastic algorithm. *Chem. Eng. Res. Des.* **2019**, *145*, 48–52. [CrossRef]
15. Cui, C.; Zhang, Q.; Zhang, X.; Sun, J. Eliminating the vapor split in dividing wall columns through controllable double liquid-only side-stream distillation configuration. *Sep. Purif. Technol.* **2020**, *242*, 116837. [CrossRef]
16. Zhang, T.; Li, M.; Pan, H.; Ling, H. Dynamic control of liquid-only transfer Kaibel dividing-wall column. *Chem. Eng. Sci.* **2023**, *272*, 118589. [CrossRef]
17. Qu, X.C.; Wu, Y.Y.; Zhu, J.W.; Chen, K.; Wu, B.; Ji, L.J. Separation of ternary system (1,2-ethanediol+1,3-butanediol+1,3-propanediol) by distillation. *Sep. Sci. Technol.* **2018**, *53*, 2435–2443. [CrossRef]
18. Yang, C.; Sun, Y.; Qin, Z.; Feng, Y.; Zhang, P.; Feng, X. Isobaric Vapor–Liquid Equilibrium for Four Binary Systems of Ethane-1,2-diol, Butane-1,4-diol, 2-(2-Hydroxyethoxy)ethan-1-ol, and 2-[2-(2-Hydroxyethoxy)ethoxy]ethanol at 10.0 kPa, 20.0 kPa, and 40.0 kPa. *J. Chem. Eng. Data* **2014**, *59*, 1273–1280. [CrossRef]
19. Wilson, G.M. Vapor-liquid equilibrium. XI. A new expression for the excess free energy of mixing. *J. Am. Chem. Soc.* **1964**, *86*, 127–130. [CrossRef]
20. Renon, H.; Prausnitz, J.M. Local compositions in thermodynamic excess functions for liquid mixtures. *AIChE J.* **1968**, *14*, 135–144. [CrossRef]
21. Abrams, D.S.; Prausnitz, J.M. Statistical thermodynamics of liquid mixtures: A new expression for the excess Gibbs energy of partly or completely miscible systems. *AIChE J.* **1975**, *21*, 116–128. [CrossRef]
22. Rodrigues, M.; Francesconi, A.Z. Experimental Study of the Excess Molar Volumes of Binary and Ternary Mixtures Containing Water +(1,2-Ethanediol, or 1,2-Propanediol, or 1,3-Propanediol, or 1,2-Butanediol) + (1-n-Butyl-3-methylimidazolium Bromide) at 298.15 K and Atmospheric Pressure. *J. Solut. Chem.* **2011**, *40*, 1863–1873. [CrossRef]
23. Zhang, K.; Meng, X.Y.; Wu, J.T. Flammability Limits of Binary Mixtures of 1,2-Ethanediol plus Steam and 1,2-Propanediol plus Steam. *J. Chem. Eng. Data* **2013**, *58*, 2681–2686. [CrossRef]
24. Lin, Y.F.; Tu, C.H. Isobaric vapor-liquid equilibria for the binary and ternary mixtures of 2-propanol, water, and 1,3-propanediol at P = 101.3 kPa: Effect of the 1,3-propanediol addition. *Fluid Phase Equilib.* **2014**, *368*, 104–111. [CrossRef]
25. Zhong, Y.; Wu, Y.Y.; Zhu, J.W.; Chen, K.; Wu, B.; Ji, L.J.; Shen, Y.L. The Distillation Process Design for the Ternary System 1,2-Butanediol + 1,4-Butanediol + 2,3-Butanediol. *Sep. Sci. Technol.* **2015**, *50*, 2545–2552. [CrossRef]

26. Zhai, X.; Wu, Y.; Tian, B.; Yao, Y.; Wu, B.; Chen, K.; Ji, L. Isobaric Vapor-Liquid Equilibrium for the Binary System of Cumene plus Acetophenone at 101.3, 30.0, and 10.0 kPa. *J. Chem. Eng. Data* **2022**, *67*, 669–675. [CrossRef]
27. Yi, Q.; Chen, W.P.; Zhang, X.Y.; Wu, Y.Y.; Wu, B.; Chen, K.; Ji, L.J. Isobaric Vapor–Liquid Equilibrium for the Binary Systems of 2-Phenylethanol + 2-Ethylphenol, 1-Phenyl-2-propanol + 2-Ethylphenol, 2-Phenylethanol + 1-Phenyl-2-propanol and 2-Phenyl-1-propanol + 2-Ethylphenol under 101.3 kPa. *J. Chem. Eng. Data* **2021**, *66*, 4351–4360. [CrossRef]
28. Chen, M.; Yu, N.; Cong, L.; Wang, J.; Zhu, M.; Sun, L. Design and Control of a Heat Pump-Assisted Azeotropic Dividing Wall Column for EDA/Water Separation. *Ind. Eng. Chem. Res.* **2017**, *56*, 9770–9777. [CrossRef]
29. Lee, H.-Y.; Yeh, M.-H.; Chen, Y.-Y.; Chen, C.-L. Design and control of a comprehensive Ethylenediamine (EDA) process with external/internal heat integration. *Sep. Purif. Technol.* **2022**, *293*, 121137. [CrossRef]
30. Liu, Y.; Zhai, J.; Li, L.; Sun, L.; Zhai, C. Heat pump assisted reactive and azeotropic distillations in dividing wall columns. *Chem. Eng. Process. Process Intensif.* **2015**, *95*, 289–301. [CrossRef]
31. Douglas, J.M. *Conceptual Design of Chemical Processes*; McGraw-Hill: New York, NY, USA, 1988.
32. Zheng, H.; Luo, X.; Yin, G.; Chen, J.; Zhao, S. Vapor Pressure and Isobaric Vapor–Liquid Equilibrium for Binary Systems of Furfural, 2-Acetylfuran, and 5-Methylfurfural at 3.60 and 5.18 kPa. *J. Chem. Eng. Data* **2018**, *63*, 49–56. [CrossRef]
33. Redlich, O.; Kister, A.T. Thermodynamics of Nonelectrolyte Solutions-x-y-t relations in a Binary System. *Ind. Eng. Chem. Res.* **1948**, *40*, 341–345. [CrossRef]
34. Fredenslund, A.; Gmehling, J.; Rasmussen, P. *Vapor–Liquid Equilibria Using UNIFAC—A Group Contribution Model*; Elsevier: Amsterdam, The Netehrlands, 1977.
35. Mathias, P.M. Effect of VLE uncertainties on the design of separation sequences by distillation—Study of the benzene–chloroform–acetone system. *Fluid Phase Equilib.* **2016**, *408*, 265–272. [CrossRef]
36. Sosa, A.; Ortega, J.; Fernández, L.; Pacheco, J.M.; Wisniak, J.; Romero, A. Further Advance to a Practical Methodology to Assess Vapor–Liquid Equilibrium Data: Influence on Binaries Rectification. *J. Chem. Eng. Data* **2019**, *64*, 3933–3944. [CrossRef]
37. Kiss, A.A. *Advanced Distillation Technologies: Design, Control, and Applications*; Wiley: Chichester, UK, 2013.
38. Cui, C.; Li, X.; Guo, D.; Sun, J. Towards energy efficient styrene distillation scheme: From grassroots design to retrofit. *Energy* **2017**, *134*, 193–205. [CrossRef]
39. Luyben, W.L. *Distillation Design and Control Using Aspen™ Simulation*; John Wiley & Sons, Inc.: Hoboken, NY, USA, 2013.
40. Song, Z.-W.; Cui, W.; Wu, Y.-Y.; Wu, B.; Chen, K.; Ji, L.-J. Energy, exergy, economic, and environmental analysis of a novel liquid-only transfer dividing wall column with vapor recompression. *Sep. Purif. Technol.* **2024**, *329*, 125122. [CrossRef]
41. Li, Q.; Feng, Z.; Rangaiah, G.P.; Dong, L. Process Optimization of Heat-Integrated Extractive Dividing-Wall Columns for Energy-Saving Separation of CO_2 and Hydrocarbons. *Ind. Eng. Chem. Res.* **2020**, *59*, 11000–11011. [CrossRef]
42. Sun, L.-Y.; Chang, X.-W.; Qi, C.-X.; Li, Q.-S. Implementation of Ethanol Dehydration Using Dividing-Wall Heterogeneous Azeotropic Distillation Column. *Sep. Sci. Technol.* **2011**, *46*, 1365–1375. [CrossRef]
43. Sun, L.; Wang, Q.; Li, L.; Zhai, J.; Liu, Y. Design and Control of Extractive Dividing Wall Column for Separating Benzene/Cyclohexane Mixtures. *Ind. Eng. Chem. Res.* **2014**, *53*, 8120–8131. [CrossRef]

Disclaimer/Publisher's Note: The statements, opinions and data contained in all publications are solely those of the individual author(s) and contributor(s) and not of MDPI and/or the editor(s). MDPI and/or the editor(s) disclaim responsibility for any injury to people or property resulting from any ideas, methods, instructions or products referred to in the content.